PAPER

Check for updates

Cellulose acetate composites with bamboo cellulose nanofibers: crystallinity preservation during tetrabutylammonium salt-catalyzed surface acetylation

Hao Wang, [a] Kyoya Shirotani,[a] Naoki Wada [*b] and Kenji Takahashi [*b]

Conventional ionic liquids (ILs) used for cellulose modification, while effective in dissolving cellulose, often induce a transition from the robust cellulose I crystalline structure to the weaker cellulose II crystalline phase, compromising material strength. To overcome this limitation, we developed six types of tetrabutylammonium (TBA)-based organic salts, including TBA acetate, aimed at modifying the cellulose surface while preserving its native crystalline structure. Regenerated cellulose nanofibers (CNFs) treated with these TBA-based salts were analyzed *via* X-ray diffraction and scanning electron microscopy, revealing that TBA maleate minimally affected crystallinity and retained the cellulose I crystalline structure. Subsequently, TBA maleate was employed as the solvent medium for the surface modification (acetylation) of CNFs, achieving a degree of substitution of 0.5. The modified CNF acetate (CNF-ac) was blended with commercial cellulose acetate (CA) at ratios of 1, 3, and 5 wt% to evaluate its reinforcing potential. The cellulose I-rich CNF derivative exhibited superior dispersion within the CA matrix, leading to a 46% enhancement in mechanical properties. Overall, this study highlights the potential of crystalline structure-preserving organic salts for the development of high-performance cellulose-based composite materials.

Introduction

In recent years, plastic pollution and resource depletion have become significant global environmental issues. Between 1950 and 2015, 6.3 billion tons of plastic waste were produced globally, including both primary and recycled materials. Of this, approximately 9% is recycled, 12% is incinerated, and the remaining 79% is either in landfills or released directly into the environment.[1] Due to their poor biodegradability, petroleum-based plastics accumulate in the environment over the long term, causing severe damage to ecosystems.[2] The limited availability of petroleum resources has exacerbated this crisis. Consequently, the development of alternative materials derived from renewable resources has become a critical research focus. Among these candidates, cellulose has demonstrated immense potential, owing to its abundant availability, renewability, biodegradability, and excellent mechanical properties.[3–5] As the most abundant bio-based polymer in nature, the development and utilization of cellulose not only reduce the reliance on petroleum resources but also offer new pathways for constructing environmentally friendly materials.

Due to its high molecular weight and the presence of robust intra- and intermolecular hydrogen-bonding networks, cellulose exhibits low solubility in conventional single-component solvents and cannot be processed by melting. These characteristics present significant challenges for fabricating functional cellulose-based structures. Conventionally, heterogeneous systems have been employed for chemical modification without fully dissolving cellulose,[6] enabling the production of derivatives with improved solubility and thermoplastic properties, such as cellulose esters soluble in various organic solvents.

Considerable research has therefore been dedicated to identifying solvent systems capable of directly dissolving cellulose, thereby enabling its direct processing into fibers, films, and composites, while also facilitating greener and more controlled homogeneous chemical modifications. Various aqueous solvent systems have been investigated, including inorganic metal complex solutions (*e.g.*, cuprammonium hydroxide), molten inorganic salt hydrates (*e.g.*, $LiCl \cdot 5H_2O$), and alkali hydroxide-based solutions (*e.g.*, $NaOH/urea/H_2O$). Non-aqueous alternatives such as DMA/LiCl and DMSO/TBAF have also been explored, as well as derivatization-based approaches, including the viscose process (cellulose xanthate) or the use of DMF and DMSO with N_2O_4.[7] However, these solvent systems often suffer from drawbacks, such as toxicity, poor recyclability, and instability, which have been widely acknowledged and critically analyzed.

aGraduate School of Natural Science and Technology, Kanazawa University, Japan
bInstitute of Science and Engineering, Kanazawa University, Kanazawa, Japan. E-mail: naoki-wada@se.kanazawa-u.ac.jp; ktkenji@staff.kanazawa-u.ac.jp

The emergence of ionic liquids (ILs) as direct, tunable solvents for cellulose has significantly advanced this field, leading to novel materials with unprecedented properties.[8,9] ILs are liquid salts comprising organic cations paired with organic or inorganic anions. Owing to their unique physicochemical profiles, ILs exhibit near-zero vapor pressures, eliminating volatility concerns while maintaining exceptional thermal and chemical robustness under operational conditions.[10,11] Incorporating aprotic cosolvents such as DMSO or DMF into ILs can improve their ability to dissolve cellulose under mild conditions.[12,13] However, most ILs induce a crystalline transformation from cellulose I (natural form) to cellulose II during dissolution, accompanied by a decrease in the crystallinity index. The resulting materials are typically more amorphous, with significantly diminished mechanical properties.[14] Although these systems are effective in dissolving cellulose, their inability to preserve the crystalline structure limits their suitability for high-performance applications.

In this study, we focus on the molecular design of tetrabutylammonium ([TBA]$^+$)-based salts and their potential applications in cellulose processing and catalytic conversion. The selection of [TBA]$^+$ as the cationic core is primarily driven by its unique steric hindrance effect and dynamic stability regulation.[15]

At the anion design level, seven carboxylate anions—citrate, succinate, fumarate, acetate, oxalate, malonate, and maleate (Fig. 1)—were selected to construct an anion library characterized by renewability, molecular size gradients, and functional complementarity. Citric acid is produced industrially via citrus extraction or microbial fermentation,[16] whereas succinic acid (Suc), a key bio-based platform chemical, is synthesized via microbial fermentation of glucose.[17] Fumaric acid (Fum) occurs naturally as an intermediate of the tricarboxylic acid cycle and can also be obtained by fungal fermentation.[18] Acetic acid is widely available from biomass-based fermentation processes,[19] whereas oxalic acid can be directly extracted from plants such as spinach and sugar beet.[20,21] Conversely, malonic acid occurs only in trace amounts in nature as a transient metabolic intermediate and is primarily produced via green chemical

synthesis,[22] whereas maleic acid is rarely found naturally and is primarily obtained via catalytic oxidation of bio-based or petroleum-derived feedstocks.[23] From a molecular engineering perspective, independent of their bio-source, the gradient design of anion size and functional groups enables precise regulation of cellulose dissolution performance. Small carboxylate anions (acetate, oxalate, and malonate), with their high charge density and low viscosity, can rapidly penetrate the cellulose microfibril gaps to selectively cleave intramolecular hydrogen bonds. Medium-sized anions (maleate, succinate, and fumarate) balance dissolution efficiency and steric hindrance via their C4 chain lengths, where the cis-double bond configuration of maleate enhances the polar affinity with the cellulose hydroxyl groups, while the trans-conformation of fumarate provides additional thermodynamic stability to the system. Larger citrate anions leverage their tricarboxylate groups and hydroxyl multi-site coordination capabilities to achieve strong complexation of highly crystalline cellulose. The strategic selection of anions thus enables control over the dissolution capacity of the cellulose crystalline regions.

Among the various forms of cellulose that benefit from surface modification, cellulose nanofibers (CNFs) are particularly attractive owing to their excellent mechanical properties and versatility in composite applications. CNFs can be obtained through mechanical disintegration of cellulose fibers or wood pulp, typically exhibiting lengths of several micrometers and diameters ranging from 5 to 100 nm. Compared with cellulose nanocrystals (CNCs), CNFs offer a higher aspect ratio, lower critical concentration for percolation network formation, and lower production cost, making them ideal candidates for reinforcing fillers in polymer matrices.[24] Accordingly, CNFs have been widely studied and incorporated as fillers into bio-based polymeric materials such as cellulose acetate butyrate (CAB).[25] However, due to their intrinsically hydrophilic surfaces, CNFs are only compatible with hydrophilic polymer matrices and are readily used as reinforcement agents in hydrophilic resins such as poly(ethylene oxide) (PEO) and poly(vinyl alcohol) (PVA). Their hydrophilic nature significantly limits their application as reinforcement for hydrophobic polymers such as polypropylene (PP) and polyethylene (PE). The incompatibility between the apolar polymer matrices and polar CNF surface leads to poor dispersion and the formation of CNF agglomerates, which severely hinders the performance of the composites.[26] To improve compatibility with hydrophobic polymers, surface modification of CNF is essential to reduce hydrogen bonding and van der Waals forces between fibers while optimizing wettability with polymeric resins. Rol et al. reviewed recent advances in CNF surface modification, highlighting their value in material reinforcement and industrial applications.[27]

Previous studies have shown that a degree of substitution (DS) of approximately 0.5 preserves the native fiber morphology of CNFs, while still providing reinforcement in various matrices.[28,29] Based on this finding, we synthesized CA with a DS of approximately 0.5 as a reinforcing agent. To explore the effects of surface modification on the performance of the CNF composites, CA/CNF nanocomposites were prepared, including both unmodified and surface-acetylated CNFs. Their
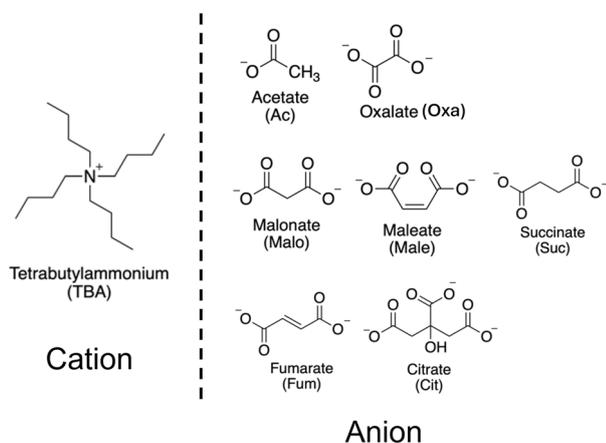

Fig. 1 Chemical structure of the tetrabutylammonium-based salts utilized in this study.

morphological characteristics, rheological properties, and crystallization behavior were analyzed in detail. Furthermore, the cellulose-based nanocomposites were fabricated *via* direct melt processing, which is considered a more economical and industrially viable technique than solution casting, particularly for high-volume production.

Overall, this study contributes to the development of high-performance cellulose-based composites by introducing a novel organic salt for cellulose surface modification. Our findings provide both fundamental insights and technical support for addressing plastic pollution and resource depletion, while advancing the industrialization of cellulose-based nanocomposites.

Experimental

Materials

Commercial cellulose acetates were supplied by MP Gokyo Food & Chemical Co., Ltd (Japan). Bamboo CNF was obtained from Chuetsu Pulp & Paper Co., Ltd (Japan). TBA acetate and TBAOH were purchased from Tokyo Chemical Industry Co., Ltd (Japan). Additional chemical reagents used for IL synthesis were sourced from multiple suppliers (Kanto Chemical Co., Inc., Tokyo Chemical Industry Co., Ltd, Nacalai Tesque, Inc., and Fujifilm Wako Pure Chemical Co., Ltd, Japan). Dimethyl sulfoxide (DMSO) and isopropenyl acetate were purchased from KANTO CHEMICAL Co., Inc (Japan).

Synthesis of TBA-based salts

TBA-based salts were synthesized *via* a neutralization method. Upon magnetic stirring at 25 °C, a 1.59 M aqueous solution of TBA hydroxide (TBAOH, 10 mL) was mixed with a stoichiometrically equivalent acid solution of a predetermined concentration. The acid was added dropwise to the TBAOH solution. Following completion of the reaction, the homogeneous mixture was aliquoted into glass vials, flash-frozen in liquid nitrogen, and lyophilized for 24–48 h to remove the residual water. The final products were stored in a nitrogen-purged glovebox. Structural identification was performed *via* ^{1}H NMR and ^{13}C NMR spectroscopy in deuterated water (D$_2$O), with integration ratio analysis confirming the stoichiometry of the target product.

Effects of TBA-based salts on CNF crystallinity

The effects of the synthesized TBA-based salts on the CNF structure were investigated using a fiber-redispersion protocol, where DMSO was used as a cosolvent.[30] Organic salt/DMSO mixed solvents (3 : 97) were prepared by combining each salt with DMSO in a 50 mL vial within a nitrogen-purged glove box. 0.1 g of freeze-dried CNFs was added to the solvent mixture. The suspension was stirred at room temperature until the aggregates were fully dispersed, followed by continuous stirring at 80 °C for 3 h. After fiber-redispersion, polarized optical microscopy images of CNF in the seven organic salt systems were obtained.

Following TBA-salt/DMSO treatment, 40 mL of methanol (MeOH) was introduced to induce precipitation, followed by the addition of 100 mL of MeOH after visual confirmation of product formation. The mixture was stirred at room temperature for 30 min and allowed to settle. The salt/DMSO/CNF/MeOH slurry was vacuum-filtered through a 0.45 μm PTFE membrane, and the recovered CNF was dried under reduced pressure at 70 °C for 24 h (Fig. S1). The crystallinity index (CI) was determined *via* powder X-ray diffraction using the empirical method described by Park *et al.*[31]

XRD analysis revealed that the regenerated bamboo CNFs maintained favorable crystallinity, with the cellulose I crystalline structure being particularly well-preserved. Four regenerated CNF samples exhibiting the highest CI values were selected for systematic morphological characterization *via* scanning electron microscopy (SEM). The different TBA-based salt systems were evaluated for their effects on cellulose crystallinity during fiber-redispersion, through a comparative analysis of the fiber structural integrity, including dispersion state, surface topography, and potential aggregation phenomena. This comprehensive approach enabled the identification of organic salts that not only effectively promote the reaction but also minimally impact the intrinsic crystallinity of cellulose.

Acetylation of CNF using TBA-based salts

Investigation of CNF acetylation reactions using the synthesized salts involved observation of CNF surface morphological changes *via* microscopy to identify the most effective candidate. The solvent composition was TBA-salt:DMSO : MeCN = 2 : 6 : 92 (w/w), with a bamboo CNF concentration of 2.5 wt% relative to the solvent mixture. Isopropyl acetate was used as the acetylation reagent at 1 eq. relative to the hydroxyl groups of cellulose (Scheme 1). The acetylation reaction was carried out in a batch reaction, and the total solvent mass was fixed at 20 g, consisting of TBA-salt (0.4 g), DMSO (1.2 g), and MeCN (18.4 g). Bamboo CNFs (0.5 g) were dispersed in the solvent mixture under stirring at 40 °C for 30 min to form a suspension. Isopropenyl acetate (0.93 g) was then added, and the reaction was allowed to proceed at 40 °C for 2 h under continuous stirring. Upon completion, the reaction mixture was poured into 400 mL of methanol to precipitate the product, which was subsequently collected and dried under vacuum at 70 °C. Bamboo CNFs were successfully surface-modified to a DS of 0.51, while preserving their structural integrity. DS was determined *via* benzoylation of the sample (Scheme S1 and Fig. S2).

Preparation of reinforced CA films

Despite overcoming kinetic limitations, the recovered CNF-ac exhibited incompatibility when directly blended with the plasticizer-containing cellulose acetate CA (DS = 2.2), affording
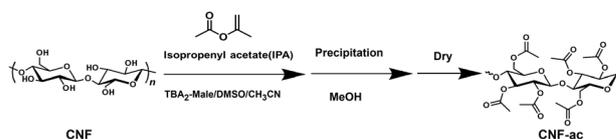
Scheme 1 Surface acetylation of bamboo CNFs.

non-uniform films. To address this issue, CNF-ac was premixed with plasticizer-free CA (DS = 2.2) in solution to form a masterbatch prior to recovery. Specifically, plasticizer-free CA—equivalent to the theoretical product mass—was introduced into the reaction system to enhance interfacial compatibility. Methanol-induced precipitation was then employed to obtain a homogenized 50 : 50 (w/w) masterbatch consisting of plasticizer-free CA and the modified CNF-ac. During film processing, precise stoichiometric compensation was achieved by blending this masterbatch with CA containing 28% plasticizer (compared with 22% in the control group), ensuring an identical final plasticizer content across all samples while maintaining chemical homogeneity. Composite films incorporating 1%, 3%, 5%, 10%, and 20% CNF-ac were fabricated *via* hot pressing. Parallel control films containing unmodified bamboo CNFs were prepared using identical processing conditions. This methodology maintained a constant plasticizer content and processing parameters, thereby effectively isolating the influence of substituents on the performance mechanism of the material. The resulting film series establishes a chemically coherent platform for probing the structure–property relationships in surface-modified cellulose-based composites, while the CNF-based controls enable clear differentiation between substitution-specific effects and generic reinforcement behavior.

Fourier transform infrared (FT-IR) spectroscopy

Fourier Transform Infrared (FT-IR) spectroscopy was performed using a Nicolet iS10 spectrometer (Thermo Fisher Scientific Inc.) equipped with a DTGS KBr detector and an attenuated total reflectance (ATR) unit. Spectra were collected over the 4000–400 cm^{-1} range at a resolution of 4 cm^{-1}, with 64 scans accumulated to ensure a high signal-to-noise ratio (S/N) of 35 000 : 1.

NMR and degree of substitution

The substitution characteristics (degree and distribution patterns) of cellulose esters were quantitatively analyzed using a high-resolution nuclear magnetic resonance (NMR) spectrometer (JNM-ECA 600, JEOL Ltd, Tokyo, Japan). Two distinct internal reference systems were employed: trimethylsilyl propanesulfonic acid-d$_6$ (TSPS-d$_6$) for TBA-based salts and tetramethylsilane (TMS) for CNF ester derivatives.

^{1}H NMR spectra were acquired under standardized analytical conditions (operating frequency, 600 MHz; temperature, 298 K; accumulated scans, 64) to ensure signal-to-noise ratio optimization. Spectral deconvolution and peak integration were performed using Delta NMR software (v5.3, JEOL Ltd) with chemical shifts referenced to residual solvent peaks.

Scanning electron microscopy (SEM) and polarized light microscopy

SEM sample preparation followed a standardized protocol to ensure surface conductivity and morphological preservation. The specimens were secured on a planar sample stage with conductive carbon adhesive tape, followed by the deposition of a 5 nm Au/Pd alloy coating using a precision magnetron sputter coater (E−1030, Hitachi Ltd, Tokyo, Japan). Sputtering was conducted at a chamber pressure of 6 Pa, DC current, and a deposition time of 40 s, achieving uniform nanoscale metallic coverage without thermally induced structural deformation. High-resolution images were acquired using a field-emission scanning electron microscope (JSM-6510LV; JEOL Ltd, Tokyo, Japan) operating at an acceleration voltage of 10 kV.

Polarized light microscopy observations were conducted using an MT9430L system (MEIJI TECHNO Co., Ltd) equipped with a first-order red compensator. Imaging was performed at a ×200 objective magnification to analyze the sample features with enhanced optical contrast and crystalline orientation sensitivity under cross-polarized conditions.

X-ray diffraction (XRD) spectroscopy

X-ray diffraction (XRD) analysis of both regenerated CNFs and surface-modified CNFs was conducted using a MiniFlex 600 diffractometer (Rigaku Co., Ltd, Japan) equipped with a Cu–Kα radiation source (λ = 1.5418 Å) operated at 40 kV and 10 mA. Scattering patterns were collected over a 2θ range of 5° to 50° with a scanning rate of 10° min^{-1} under ambient conditions. The crystallinity of the materials was determined using the peak height method described by Segal.[32] The crystallinity index (C.I.) was evaluated using the crystalline intensity peak of the 200 planes ($I_{22.5}$) and the minimum intensity of the amorphous region (I_{18}) between the 200 and 110 planes, according to the following equation:

$$\text{C.I}(\%) = \frac{I_{22.5} - I_{18}}{I_{22.5}} \times 100$$

Thermal analysis and tensile test

Thermal processability was evaluated using a capillary rheometer flow tester (CFT-500EX, Shimadzu Corp., Kyoto, Japan). The dried sample (1.0 g) was placed into the barrel and compressed by a piston with a diameter of 10 mm. The sample was preheated to 50 °C for 60 s, after which a constant pressure of 4.9 MPa was applied to the piston at a heating rate of 3 °C min^{-1}. T_{offset} was determined as the temperature at which the piston descended by 5 mm due to the melt flow of the sample. For CA containing 22% plasticizer, the T_{offset} was determined to be 180 °C.

For film fabrication, masterbatches were processed *via* hot pressing. Dried samples (2.0 g) were placed on the aluminum plate of the hot press machine, with the heating temperature set to 190 °C (T_{offset} + 10 °C). The samples were preheated for 5 min under a pressure of 0 kN and then pressed at 60 kN for 3 min. After pressing, the films were allowed to cool, and dumbbell-shaped specimens were cut using a punching machine (IMC-1948, Imoto Machinery Co., Kyoto) in accordance with the JIS K7139 standards. Tensile testing was performed to evaluate the mechanical properties of the films using a universal testing machine specifically designed for thin films (EZ-SX; Shimadzu Corp., Kyoto, Japan). The tensile properties of each sample were calculated as the average of at least three measurements.

Results and discussion

Analysis of the synthesized TBA-based salts

Structural validation of the synthesized salts was conducted *via* comprehensive NMR analyses, as shown in Fig. S3–S9. ^{1}H NMR spectra were acquired using trimethylsilyl propanesulfonic acid-d6 (TSPS-d6, 0.05 wt% in D$_2$O) as the internal standard under fully deuterated conditions. For TBA$_2$-oxa (Fig. S3), no ^{1}H signals originating from the anion were observed owing to the proton-deficient nature of oxalate; however, its presence was confirmed by a characteristic ^{13}C resonance at δ 173.46 ppm.

(Fig. S9). TBA$_2$-Malo (Fig. S4) exhibited a characteristic singlet peak corresponding to methylene protons at δ 3.10 ppm. In the case of TBA$_2$-Male (Fig. S5), vinyl proton signals appeared at δ 6.05 ppm, consistent with a *cis*-coupled alkene system. By contrast, TBA$_2$-Fum (Fig. S7) showed a *trans*-coupled vinyl proton doublet at δ 6.51 ppm, enabling clear differentiation between the geometric isomers. TBA$_2$-Suc (Fig. S6) displayed a distinct singlet assigned to methylene protons at δ 2.36–2.42 ppm, while TBA$_3$-Cit (Fig. S8) showed equivalent methylene proton resonances at δ 2.62–2.65 ppm, confirming retention of the tricarboxylate framework. This multinuclear (^{1}H and ^{13}C) approach systematically verified both cationic integrity and anionic fidelity across all synthesized salts. The absence of extraneous peaks and the quantitative integration ratios (TBA : anion = 1 : 1) further validated the chemical purity and stoichiometric precision of the ionic pairs.
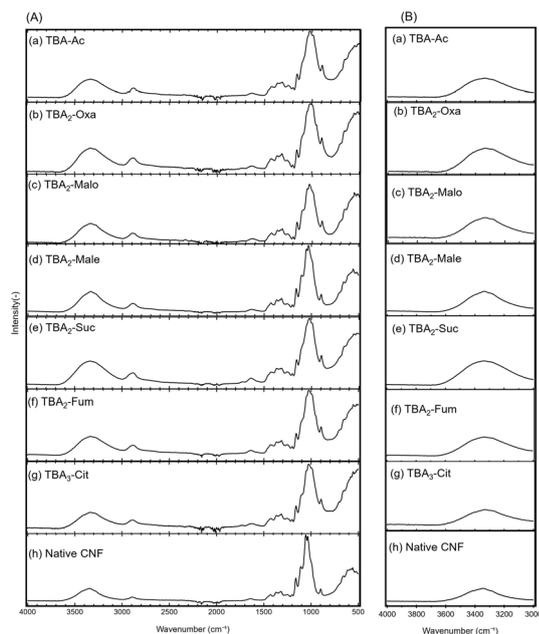
FT-IR analysis of regenerated bamboo CNFs

The FT-IR spectra of the regenerated bamboo CNFs treated with seven TBA-based salts, together with native CNFs (Fig. 2), provided critical insights into the structural modifications. In the hydroxyl stretching region (3000–4000 cm^{-1}, expanded in Fig. 2B), native CNFs exhibited a broad OH band at $\sim$3350 cm^{-1}, attributed to strong intra- and intermolecular hydrogen bonding within the cellulose matrix.[33] The regenerated CNF samples (a–g) exhibited shifts in the OH peak position and narrowing of the absorption band, indicating the partial disruption of hydrogen bonds. The TBA-Ac (a), TBA$_2$-Oxa (b), and TBA$_2$-Malo (c) samples exhibited a slight downshift to $\sim$3320 cm^{-1}, suggesting moderate hydrogen bond cleavage facilitated by interactions with anions.

Fig. 2 (A) FT-IR spectra of the regenerated bamboo CNFs and (B) expanded spectra of the hydroxyl groups using (a) TBA-Ac, (b) TBA$_2$-Oxa, (c) TBA$_2$-Malo, (d) TBA$_2$-Male, (e) TBA$_2$-Suc, (f) TBA$_2$-Fum, (g) TBA$_3$-Cit, and (h) FT-IR spectrum of the native bamboo CNF.

Characterization of CNF crystallinity

XRD analysis was systematically conducted to evaluate the crystalline reorganization of the regenerated CNFs under
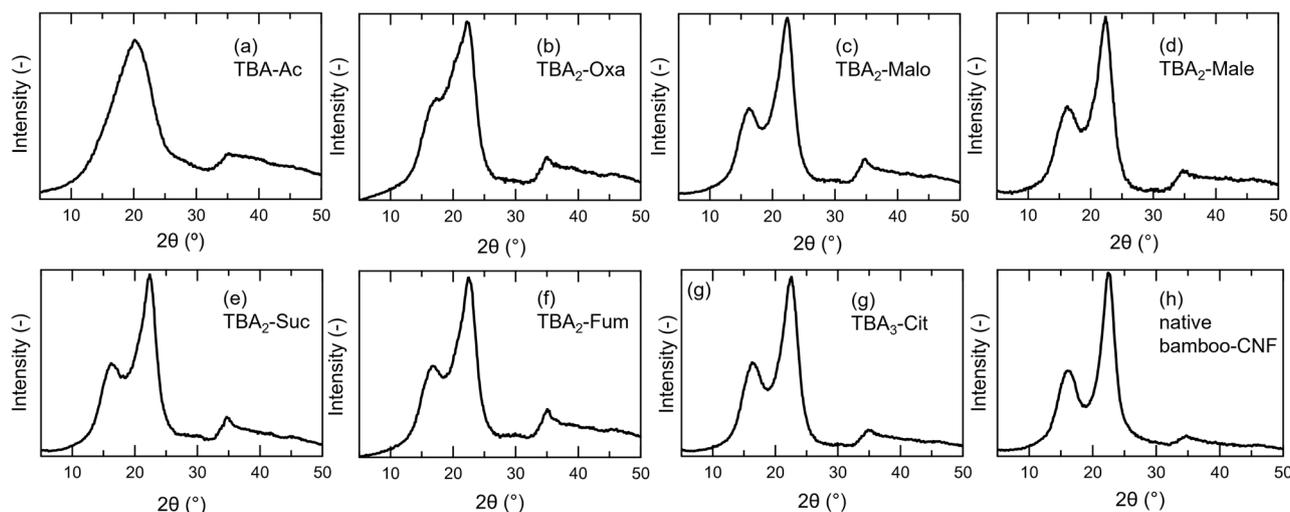

Fig. 3 XRD spectra of bamboo CNFs regenerated from various TBA-based salts and DMSO mixtures; (a) TBA-Ac, (b) TBA$_2$-Oxa, (c) TBA$_2$-Malo, (d) TBA$_2$-Male, (e) TBA$_2$-Suc, (f) TBA$_2$-Fum, (g) TBA$_3$-Cit, and (h) native bamboo-CNFs.

Table 1 Crystallinity index of bamboo-CNFs re-generated from various TBA-based salts and DMSO mixtures (3/97 w/w)

Run	TBA-based salt	C.I^a	Intact crystal^b (%)
1	TBA-Ac	0.47	67
2	TBA$_2$-Oxa	0.42	60
3	TBA$_2$-Malo	0.61	87
4	TBA$_2$-Male	0.61	87
5	TBA$_2$-Suc	0.55	79
6	TBA$_2$-Fum	0.55	79
7	TBA$_3$-Cit	0.71	100

^{a} C.I. values were evaluated using the Segal method. ^{b} The C.I. value of native bamboo CNFs was 0.71. The percentage of intact crystals was calculated by comparing the C.I. values before and after regeneration.

Fig. 4 SEM images of bamboo CNFs regenerated from various TBA-based salts and DMSO mixtures (a) TBA$_2$-Malo, (b) TBA$_2$-Male, (c) TBA-Suc, and (d) TBA$_2$-Fum.

different TBA-based salt treatments. By examining the crystalline structure of CNFs treated with TBA-Ac and the six synthesized TBA-based salts (Fig. 3), a notable difference was observed in the regenerated CNF TBA$_2$-Oxa (Fig. 3b). While retaining the characteristic Cellulose I diffraction peak at 22.5° (002 plane), an additional peak emerged at 20° corresponding to the (101) reflection of cellulose II. This suggests partial molecular-level dissolution, followed by recrystallization into a thermodynamically stable allomorph during regeneration.

Crystallinity was quantified using the Segal method (Table 1). TBA$_3$-Cit (100%) exhibited maximum crystallinity retention; however, due to potential acetylation *via* citrate hydroxyl groups, it was excluded from subsequent analyses. TBA$_2$-Male (87%) and TBA$_2$-Malo (87%) maintained viable crystalline frameworks. Conversely, TBA$_2$-Oxa (60%) and TBA-Ac (67%) showed significant de-crystallization, possibly due to anion size-dependent penetration effects.

This hierarchical crystallinity pattern correlates with the molecular dimensions of the IL anions. Smaller anions (oxalate and acetate) penetrate deeper into the cellulose matrix, disrupting hydrogen-bonding networks more effectively than their bulkier counterparts (citrate).

The differential fiber redispersion–recrystallization behavior provides critical insights for designing TBA-based salt systems that balance dissolution capacity with crystalline structure preservation.

Microscopic analysis of regenerated bamboo CNF

Following dispersion in TBA-salts/DMSO (3 : 97) mixtures at 80 °C for 3 h, polarized optical microscopic images of CNFs in the seven organic salt systems were obtained (Fig. S10). Although complete dissolution of the nanofibers was not achieved in any system, even after 3 h of treatment, pronounced differences in fiber morphology were observed. In the TBA-Ac system (Fig. S10a), CNFs almost lost their fibrous morphology, whereas in TBA$_3$-Cit (Fig. S10g), the fibrous structure was preserved.

Crystallinity analysis (Table 1) revealed that the regenerated bamboo CNFs treated with TBA$_2$-Male and TBA$_2$-Malo exhibited the highest crystallinity (87%), significantly surpassing that of the TBA$_2$-Suc and TBA$_2$-Fum systems (79%). To further elucidate the influence of TBA-based salt structures on the molecular
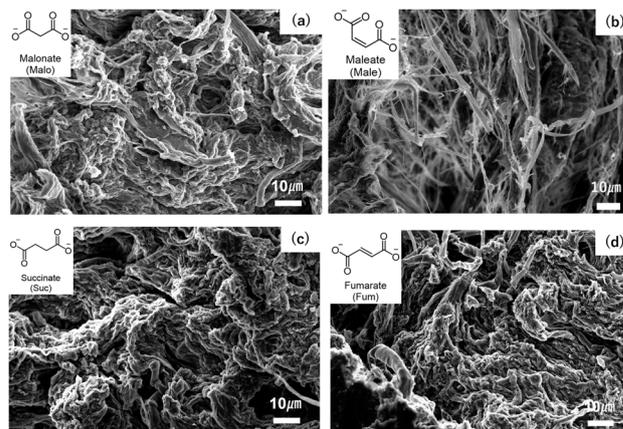
organization of cellulose, SEM was employed to characterize the morphological features of the four regenerated cellulose samples (Fig. 4). SEM imaging revealed distinct structural differences among the samples. Regenerated CNFs treated with TBA$_2$-Suc and TBA$_2$-Fum exhibited severe fiber fusion and agglomeration, accompanied by complete loss of the native tubular architecture, resulting in homogenized surfaces. While partial fiber bundle structures were retained in the TBA$_2$-Malo system, localized melting and interfacial bonding between the fibers were still evident. In contrast, the TBA$_2$-Male-treated cellulose retained well-defined fiber contours, demonstrating optimal morphological preservation.

Such morphological differences may be attributed to the spatial hindrance effects and hydrogen-bonding reconstruction capabilities of the anions. The planar rigid structure of the maleate anion (maleic acid) likely promotes an ordered dissolution environment through π–π stacking interactions, guiding the recrystallization pathways of cellulose during regeneration. Conversely, the flexible chain conformations of the Suc and Fum anions may promote the disordered rearrangement of cellulose molecular chains, leading to fiber overfusion. These findings underscore the critical role of TBA-based salts molecular design in tailoring cellulose molecular structures and provide a strategic framework for developing high-performance regenerated cellulose materials through precise anion engineering.

Solvent system design for acetylation while preserving cellulose crystallinity

When the TBA-salt/DMSO solvent system was employed, the reaction proceeded rapidly at the CNF surface. Once surface acetylation occurred, the modified cellulose chains became soluble in DMSO and detached from the fiber surface. This continuous surface dissolution exposed fresh inner fibrils, allowing the reaction to proceed inward. Consequently, the process behaved more like a dissolution–derivatization mechanism rather than a controlled surface modification. Although
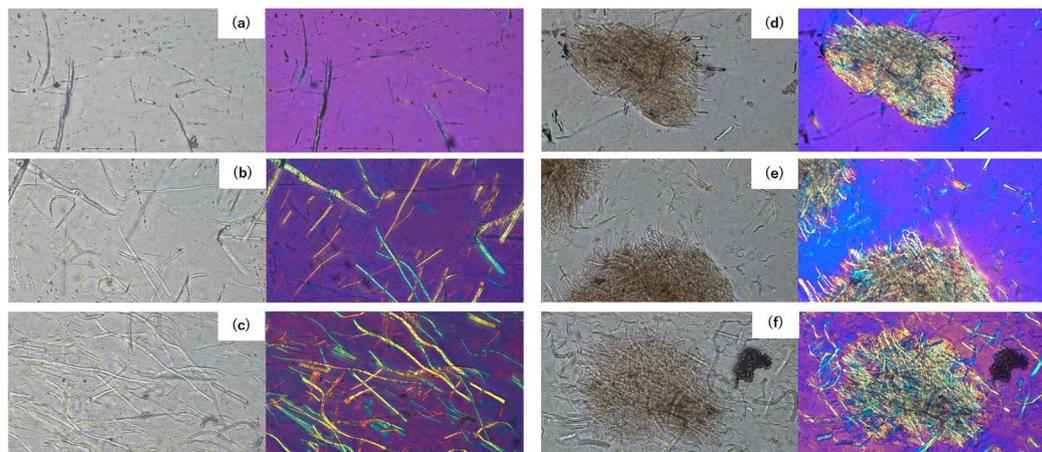
Fig. 5 Bright-field (left) and crossed-nicol (right) polarized optical micrographs of CNF-ac/CNF reinforced films. (a)–(c): commercial CA with CNF-ac. (d)–(f): commercial CA with untreated bamboo CNFs. (a) 1 wt% CNF-ac, (b) 3 wt% CNF-ac, (c) 5 wt% CNF-ac, (d) 1 wt% CNF, (e) 3 wt% CNF, and (f) 5 wt% CNF.

this promoted further acetylation, it simultaneously disrupted the native cellulose I crystalline structure, ultimately preventing its preservation. Therefore, although DMSO improves cellulose solubility, it does not enable controllable or structurally conserved acetylation, and the resulting DS cannot be regarded as representative of surface-confined modification. To address this limitation, alternative organic solvents such as THF, acetonitrile, and ethyl acetate were investigated in place of DMSO. In these systems, CNF exhibited insufficient dispersion, and acetylation was strongly suppressed, resulting in negligible DS. These observations indicate that a certain degree of anion activation by a polar solvent such as DMSO is essential for the reaction to proceed. To resolve this apparent contradiction, a ternary solvent system consisting of TBA-salt, a minimal amount of DMSO, and acetonitrile was developed. In this optimized system, DMSO is present only in a limited proportion to activate anion-catalyzed acetylation, and acetonitrile serves as the primary solvent to suppress excessive dissolution of acetylated cellulose. The optimized solvent composition (TBA-salt:DMSO:MeCN = 2:6:92 (w/w)) enabled a moderate and controllable DS to be achieved while preserving the cellulose I crystalline structure.

The XRD pattern of the surface-modified CNF-ac also indicates retention of cellulose I crystallinity (Fig. S11).

Effects of surface modification on the mechanical properties of reinforced films

The composite films reinforced with CNF-ac demonstrated superior interfacial compatibility with the plasticizer-containing CA matrix compared with the unmodified bamboo CNFs. As shown in S12 and Fig. 5 the hot-pressed films containing 1, 3, and 5 wt% CNF-ac maintained their optical transparency without macroscopic phase separation, whereas the unmodified bamboo CNF composites exhibited visible agglomerations (Fig. S12). This contrast was further confirmed by polarized light microscopy, revealing a homogeneous CNF-ac dispersion (Fig. 5a–c) *versus* particulate clusters in the control

samples (Fig. 5d–f). This enhanced compatibility originates from TBA-based salt-induced surface derivatization, which improves the chemical affinity of CNFs with the hydrophobic CA matrix through tailored interfacial interactions.

Mechanical characterization revealed concentration-dependent reinforcement effects (Fig. 6). The CNF-ac composites achieved the highest tensile strength (39.3 MPa at 5 wt%)
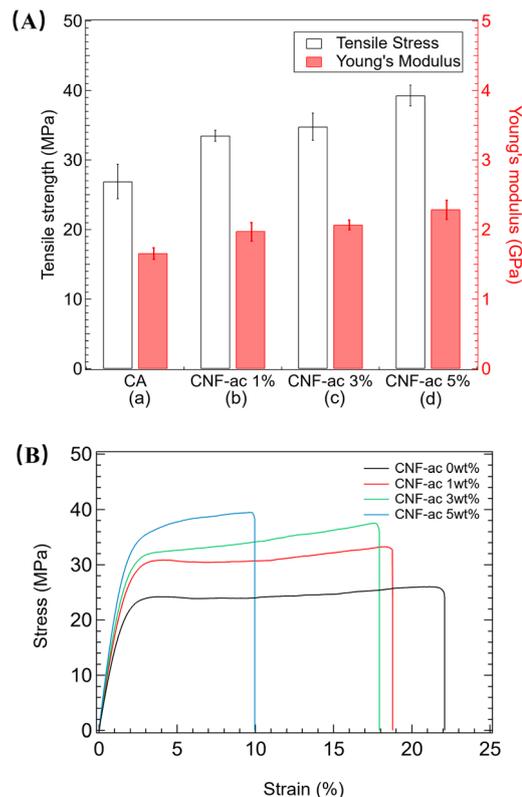

Fig. 6 Comparison of tensile test results for composite films: (A) (a) commercial CA, (b–d) CNF-ac with commercial CA (B) Stress–strain curve of cellulose acetate films reinforced with acetylated CNFs.

and Young's modulus (2.32 GPa at 5 wt%), representing 46% and 40% enhancements, respectively, over pure plasticizer-containing CA. Compared with unmodified CNFs (Fig. S13, maximum 33.8 MPa strength at 5 wt%), the performance of the CNF-ac composites suggests an optimized stress transfer efficiency through covalent/noncovalent bonding at the filler–matrix interface. Notably, the relationship between reinforcement content and ductility differed substantially between modified and unmodified systems. The CNF-ac composites maintained a higher elongation at break (18.5% at 1 wt%) than unmodified CNFs (5.49% at 1 wt%). Although higher CNF-ac loadings (10 and 20 wt%) further increased tensile strength, elongation at break decreased markedly with increasing filler content, reaching 4.95% at 20 wt% CNF-ac (Fig. S14). In contrast, films containing 10 and 20 wt% unmodified CNFs could not be processed into films suitable for tensile tests owing to severe fiber aggregation. These results suggest that surface acetylation of bamboo CNFs improves stress transfer through enhanced compatibility and interfacial interactions with the CA matrix, thereby alleviating the conventional strength–ductility trade-off observed in cellulose-based nanocomposites.

Conclusions

In this study, seven TBA-based salts, including six newly synthesized variants and the previously developed TBA-Ac, were systematically investigated for their influence on cellulose crystallinity, morphology, and catalytic performance as solvents. Among them, TBA$_2$-Male emerged as the optimal candidate for cellulose surface modification, as validated by XRD, FTIR, NMR, and SEM analyses. This organic salt enabled targeted surface modification of CNFs while preserving their native crystalline structure. To overcome the incompatibility between plasticizer-containing cellulose acetate and bamboo CNF-ac, a master-batch of CNF-ac and plasticizer-free CA (50 : 50, w/w) was developed. This masterbatch was subsequently blended with plasticizer-containing CA to make hot-pressed composite films with 1, 3, and 5 wt% CNF-ac. Comparative analyses of films containing unmodified CNFs revealed that the surface-modified CNF-ac exhibited significantly enhanced compatibility with the CA matrix, along with a measurable reinforcing effect. Microscopic evaluation and tensile testing confirmed that CNF-ac improved the mechanical properties without compromising the crystalline integrity of cellulose. These results demonstrate that TBA-maleate is a promising organic salt for tuning cellulose-derived materials, supporting its application in sustainable composites and functional materials.

Author contributions

Conceptualization: Naoki Wada, Kenji Takahashi; methodology: Naoki Wada, Kenji Takahashi; investigation: Hao Wang, Kyoya Shirotani; formal analysis: Hao Wang, Kyoya Shirotani; writing – original draft: Hao Wang; writing – review & editing: Hao Wang, Naoki Wada, Kenji Takahashi; supervision: Kenji Takahashi; all authors have read and approved the final manuscript.

Conflicts of interest

There are no conflicts to declare.

Data availability

All data supporting the findings of this study are available within the article and its supplementary information (SI) files. Supplementary information is available. See DOI: https://doi.org/10.1039/d5ra08474a.

Acknowledgements

References

1 C. J. Rhodes, *Sci. Prog.*, 2018, **101**, 201–260, DOI: 10.3184/003685018X15294876706211.

2 J. Hopewell, R. Dvorak and E. Kosior, *Philos. Trans. R. Soc., B*, 2009, **364**, 2115–2126, DOI: 10.1098/rstb.2008.0311.

3 A. F. Turbak, F. W. Snyder and K. R. Sandberg, *J. Appl. Polym. Sci.:Appl. Polym. Symp.*, 1983, **37**, 815–827.

4 A. Dufresne, *Mater. Today*, 2013, **16**, 220–227, DOI: 10.1016/j.mattod.2013.06.004.

5 M. Gericke, *et al.*, *Carbohydr. Polym.*, 2024, **326**, 121633, DOI: 10.1016/j.carbpol.2023.121633.

6 K. N. Onwukamike, S. Grelier, E. Grau, H. Cramail and M. A. R. Meier, *ACS Sustain. Chem. Eng.*, 2019, **7**, 1826–1840, DOI: 10.1021/acssuschemeng.8b04990.

7 H. Wang, G. Gurau and R. D. Rogers, *Chem. Soc. Rev.*, 2012, **41**, 1519–1537, DOI: 10.1039/C2CS15311D.

8 R. P. Swatloski, S. K. Spear, J. D. Holbrey and R. D. Rogers, *J. Am. Chem. Soc.*, 2002, **124**, 4974–4975, DOI: 10.1021/ja025790m.

9 J. Zhang, J. Wu, J. Yu, X. Zhang, J. He and J. Zhang, *Mater. Chem. Front.*, 2017, **1**, 1273–1290, DOI: 10.1039/C6QM00348F.

10 R. Farahipour, A. Mehrkesh and A. T. Karunanithi, *Environ. Sci. Pollut. Res.*, 2016, **25**, 34811–34817, DOI: 10.1016/j.ces.2015.12.015.

11 S. Suzuki and K. Takahashi, *Chem. Rec.*, 2023, **23**, e202200264, DOI: 10.1002/tcr.202200264.

12 X. Yuan and G. Cheng, *Phys. Chem. Chem. Phys.*, 2015, **17**, 31592–31600, DOI: 10.1039/C5CP05744B.

13 D. L. Minnick, R. A. Flores, M. R. DeStefano and A. M. Scurto, *J. Phys. Chem. B*, 2016, **120**, 7906–7919, DOI: 10.1021/acs.jpcb.6b04309.

14 L. Szabó, R. Milotskyi, G. Sharma and K. Takahashi, *Green Chem.*, 2023, **25**, 5338–5357, DOI: 10.1039/D2GC04730F.

15 J. Yu, L. Wang, Y. Zhao and C. Zhou, *Int. J. Biol. Macromol.*, 2021, **176**, 72–77, DOI: 10.1016/j.ijbiomac.2021.02.063.

16 M. Berovic and M. Legisa, *Biotechnol. Annu. Rev.*, 2007, **13**, 303–343, DOI: 10.1016/S1387-2656(07)13011-8.

17 H. Song and S. Y. Lee, *Enzyme Microb. Technol.*, 2006, **39**, 352–361, DOI: 10.1016/j.enzmictec.2005.11.043.

18 C. A. Roa Engel, A. J. J. Straathof, T. W. Zijlmans, W. M. van Gulik and L. A. M. van der Wielen, *Appl. Microbiol. Biotechnol.*, 2008, **78**, 379–389, DOI: 10.1007/s00253-007-1341-x.

19 R. J. Gomes, M. F. Borges, M. F. Rosa, R. J. H. Castro-Gómez and W. A. Spinosa, *Food Technol. Biotechnol.*, 2018, **56**, 139–151, DOI: 10.17113/ftb.56.02.18.5593.

20 C. F. Hanson, V. H. Frankos and W. O. Thompson, *Food Chem. Toxicol.*, 1989, **27**, 181–184, DOI: 10.1016/0278-6915(89)90067-7.

21 Y. Zheng, C. Yang, W. Pu and J. Zhang, *Food Chem.*, 2009, **114**, 1523–1528, DOI: 10.1016/j.foodchem.2008.11.021.

22 V. Ioannidou, N. Misailidis, D. Petrides and M. C. Georgiadis, *Processes*, 2024, **12**, 2559, DOI: 10.3390/pr12112559.

23 J. Blanco, M. Linares, M. López Granados, I. Agirre, I. Gandarias, P. L. Arias, J. Iglesias, J. Moreno and A. García, *Adv. Sustainable Syst.*, 2022, **6**, 2200123, DOI: 10.1002/adsu.202200121.

24 A. Isogai, *J. Wood Sci.*, 2013, **59**, 449–459, DOI: 10.1007/s10086-013-1365-z.

25 R. Milotskyi, *et al.*, *J. Compos. Sci.*, 2023, **7**, 130, DOI: 10.3390/jcs7030130.

26 L. Wang, K. Okada, M. Sodenaga, Y. Hikima, M. Ohshima, T. Sekiguchi and H. Yano, *Compos. Sci. Technol.*, 2018, **168**, 412–419, DOI: 10.1016/j.compscitech.2018.10.023.

27 F. Rol, M. N. Belgacem, A. Gandini and J. Bras, *Prog. Polym. Sci.*, 2019, **88**, 241–264, DOI: 10.1016/j.progpolymsci.2018.09.002.

28 S. Ifuku, M. Nogi, K. Abe, K. Handa, F. Nakatsubo and H. Yano, *Biomacromolecules*, 2007, **8**, 1973–1978, DOI: 10.1021/bm070113b.

29 H. Yano, H. Omura, Y. Honma, H. Okumura, H. Sano and F. Nakatsubo, *Cellulose*, 2018, **25**, 3351–3362, DOI: 10.1007/s10570-018-1787-2.

30 R. Kakuchi, R. Ito, S. Nomura, H. Abroshan, K. Ninomiya, T. Ikai, K. Maeda, H. J. Kim and K. Takahashi, *RSC Adv.*, 2017, **7**, 9423–9430, DOI: 10.1039/C6RA28659C.

31 S. Park, J. O. Baker, M. E. Himmel, P. A. Parilla and D. K. Johnson, *Biotechnol. Biofuels*, 2010, **3**, 10, DOI: 10.1186/1754-6834-3-10.

32 L. Seagl, J. J. Ceely, A. E. Martin Jr and C. M. Conrad, *Text. Res. J.*, 1959, **29**, 803–806, DOI: 10.1177/004051755902901003.

33 D. Fengel, *Holzforschung*, 1993, **47**, 103–108, DOI: 10.1515/hfsg.1993.47.2.103.